Desalination and Water Treatment
www.deswater.com

doi:10.5004/dwt.2016.0254

59 (2017) 19–30
January

Optimisation of thin film composite nanofiltration membranes based on laminated nanofibrous and nonwoven supporting material

Baturalp Yalcinkaya[a,*], Fatma Yalcinkaya[b], Jiri Chaloupek[a]

[a]*Department of Nonwoven and Nanofibrous Material, Faculty of Textile, Technical University of Liberec, Studentská 1402/2 461 17 Liberec, Czech Republic. Tel. +420777119880; email: baturalpyalcinkaya@hotmail.com (B. Yalcinkaya), Tel. +420777189301; email: yenertex@hotmail.com (F. Yalcinkaya)*
[b]*Institute for Nanomaterials, Advanced Technologies and Innovations, Technical University of Liberec, Studentská 1402/2 461 17 Liberec Czech Republic, Tel. +420777061675; email: jiri.chaloupek@tul.cz*

Received 6 March 2016; Accepted 18 June 2016

ABSTRACT

The electrospun nanofibrous membranes are one of the emerging technologies for membrane filtration; however, the applications of nanofibrous membranes hindered by their low mechanical strength and lab-scale production method. This work describes the fabrication of composite membranes consisting of the following three-layer system: a nonwoven part as the supporting material, a nanofibrous scaffold as the porous layer, and an active barrier layer. The nonwoven part and the nanofibrous scaffold were laminated together to achieve the required mechanical strength and adhesion. Formation of the active barrier layer was carried out by optimising four parameters: the monomer solution concentration, the reaction time for monomer polymerisation, the drying time and the post-treatment temperature. At each step of the process, one of the optimum conditions, indicated by filtration performance and the investigation proceeded to the next step. The filtration performance of the fabricated thin film nanofibrous composite (TFNC) membranes was done by the dead-end cell. The TFNC membrane based on m-phenylenediamine monomers showed a high rejection (93.5%) of NaCl ions at a low flux. The flux performances of the piperazine monomer-based TFNC membranes showed high $MgSO_4$ salt rejection (95.6 %) and flux at the same time.

Keywords: Nanofiltration; Interfacial polymerization; Nanofibres; Lamination; Desalination

1. Introduction

Shortages of fresh water are beginning to have grave consequences for human populations. Many countries can readily treat surface water to obtain potable water, but others are now facing water scarcity and must seek alternative water sources. One possibility for obtaining fresh water is by desalination of seawater and brackish water by membrane filtration. The membranes currently employed in water treatment processes include composite reverse osmosis (RO) membranes for water purification and nanofiltration (NF) membranes for water softening [1,2]. These membranes are multi-layered and include a selective polyamide barrier layer formed by the interfacial polymerisation (IP) of polyfunctional amine and acid chloride monomers at the interface of two immiscible solvents. The resulting thin film barrier layer separates the ions and particles in NF and RO applications [3–6]. This barrier layer is bound to supporting layers, and both layer types can be tailored independently to optimise the overall composite membrane structure and its performance characteristics, such as selectivity and permeability [7].

The physical features, chemical structure, and separation performance of composite NF membranes are well documented in the published research literature, which includes studies on the types of supporting materials [8], new monomers and their concentrations [9,10], various additives [11–13] (e.g. surfactants, ionic liquids, nanoparticles), different reaction conditions, curing temperatures and times [14], and other post-treatments. Most commercial NF

*Corresponding author.

membranes have support membranes made by a conventional phase inversion method from hydrophobic polymers like polysulfone, polyethersulfone, polycarbonate, polyphenylene oxides, polypropylene and others. However, these support membranes are typically quite thick, which usually cause a decrement in water flux.

Increases in filtration rates have now been obtained for air filtration processes through the use of filters containing nanofibrous materials [15,16]. The nanofibres provide an increased surface area and a smaller pore size; however, past and current efforts to incorporate nanofibres into liquid filtration membranes have indicated that nanofibrous layers are only effective in microfiltration and ultrafiltration processes [17,18] and are incapable of sustaining NF or RO processes.

The use of nanofibrous materials in nanofiltration has not been extensively investigated, despite the large number of studies on the production of polymeric phase-inverted membranes [5,6,8,10,11,14,19–23]. For example, Kaur et al. indicated in a number of papers that the nanofibre structure, such as its morphology, thickness and pore size, directly affects the filtration performance [24–26]. Yoon et al. reported that TFNC membranes fabricated with a polyacrylonitrile electrospun nanofibre scaffold showed a permeate flux that was two to three times greater than that obtained with conventional membranes in NF applications [27]. Wang et al. emphasised that the filtration performance (selectivity and flux) of a total membrane system consisting of a thin film (selective layer) on a nanofibre layer was determined by the thin film structure, and that this structure was considerably affected by various conditions of the IP reaction, such as different monomer concentrations [28]. Yung et al. investigated the effect of additives (e.g., ionic liquids) in the monomer solutions and found that various additives enhanced the flux without substantially compromising the rejection performance [29].

The permeation fluxes and rejection rates of currently available thin film nanofibrous composite (TFNC) membranes are comparable to those of commercial NF membranes. However, the weak mechanical properties of electrospun nanofibres and low adhesion between the supporting material (nonwoven) and the electrospun nanofibre layer pose problems for the development of liquid filters. Attempts have been made to improve the strength and integrity of the nonwoven fabric and nanofibrous scaffolds by using solvent vapor [30], applying heat and pressure [25] or by using different combinations of solvents to prepare polymer solutions for electro spinning [29,31]. All these alterations had negative influences on the morphology of the nanofibrous layer (e.g. the fibre diameter or non fibrous area increased). Moreover, these studies utilised a needle electro spinning method that is found for small-scale production of nanofibres but is an impractical method for fabrication of nanofilters on a commercial scale.

The present study investigates the possibility of using a supporting material formed from a separately fabricated bi-component polypropylene/polyethylene (PE/PP) spunbond nonwoven fabric. This layer is then coupled with a needle-free electrospun nanofibrous (polyamide 6) layer, which can be produced on a large scale, by combining the two layers gently under heat and pressure treatment using a lamination equipment.

These nanofibres, nonwoven, nonwoven and nanofibrous composite (NNC) were tested for tensile strength and pore size distribution and NNC scaffold was used as a backing material for an IP reaction to create the thin-film active barrier layer. The IP reaction itself required aqueous and organic monomers for the fabrication of thin film nanofibrous composite membranes. Even the most basic IP reactions resulted in the formation of an active barrier layer that gave high flux and rejection performance without the need for other additives (e.g. surfactants, ionic liquids, nanoparticles, etc. in the monomer solutions) or for further surface modification. All the parameters of the IP reaction for the formation of TFNC membranes were optimised, including the type of monomers, monomer concentrations, reaction time, drying time and curing temperature. Ultimately, optimised TFNC membranes were identified according to their filtration performances (selectivity and flux).

2. Experimental

2.1. Materials

The TFNC bottom substrate was a polypropylene/polyethylene (80/20, 18g m^{-2}) bi-component spunbond nonwoven fabric (Pegatex S BICO)from Pegas Nonwovens s.r.o. (Czech Republic). The solution used to produce the porous nanofibre layer by electro spinning consisted of polyamide 6 (PA6) (BASF B24) dissolved in acetic acid/formic acid. The selective layer of the TFNC membrane was prepared by interfacial polymerisation of two immiscible phases on the porous nanofibre layer. Piperazine (PIP) and m-phenylenediamine (MPD) were purchased from Sigma-Aldrich and prepared in deionised water as aqueous phases, while the organic phase was prepared by dissolving trimesoyl chloride (TMC) (Sigma-Aldrich) in hexane at 40°C. The filtration performance of TFNC membranes was tested using salt solutions containing magnesium sulphate ($MgSO_4$) and sodium chloride (NaCl).

2.2. Preparation of the electrospun PA6 porous nanofibre layer

Polyamide 6 (12 wt.%) was dissolved in acetic acid/formic acid at a ratio of 2/1 at 80°C for 4 h. This solution was then used to produce a nanofibre layer using needle-free wire electrode electro spinning equipment (NS 1WS500U, Elmarco s.r.o, Czech Republic). Wire electro spinning is a new technique that uses an electrical force to spin nanofibres from a free surface liquid towards the collector electrode (Fig. 1).

A solution carriage feeds polymer solution around a moving stainless steel wire. The speed of the carriage is 245 mm s^{-1} and the rotation speed of the wire is 40.5 cm h^{-1}. High voltage suppliers are connected to the wire electrode (55kV) and the collector electrode (–10 kV). When the applied voltage exceeds a critical value, many Taylor cones are created on the surface of the wire. Polymer solution jets move toward the collector, the solvent evaporates and the PA6 nanofibrous layer is collected on baking paper moving in front of the collector electrode. The speed of the baking paper is 9 cm min^{-1}. The distance between the electrodes is 18 cm. The temperature and humidity of input air are set to

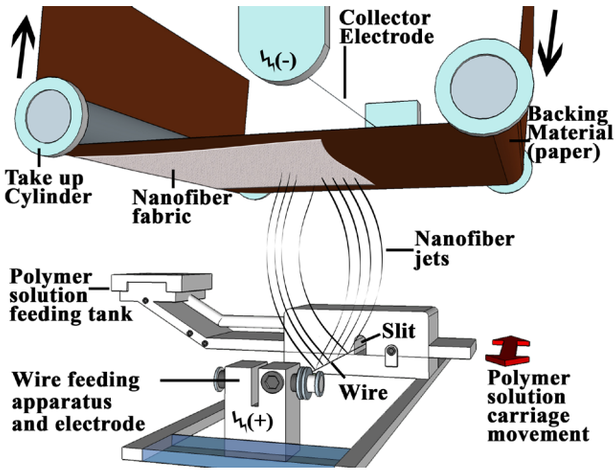

Fig. 1. Electrospinning of PA6 nanofibres using the Nanospider™ Production Line NS 1WS500U.

23°C and 30% by the air-conditioning system. The volumes of air input and output are 98 and 110 $m^3 h^{-1}$ respectively.

2.3. Lamination of the nonwoven and nanofibrous materials

Individually produced bi-component spunbond nonwoven and PA6 nanofibrous fabrics were laminated using RPS-Mini fusing lamination equipment (Meyer-Germany). This process was carried out carefully to avoid damaging the nanofibre diameter and pore size. The PA6 nanofibrous layer was put onto the PP/PE bi-component nonwoven fabric and inserted between two Teflon belts moving at 2 m min^{-1} in the lamination equipment.

The temperature was set at 135°C because of the melting point of PE (120–130°C). The nanofibrous layer was adhered to the nonwoven fabric at a pressure of 5 N cm^{-1} with the PE fibres partly melted, and the resulting product was designated the nonwoven-nanofibrous composite (NNC) scaffold (Fig. 2).

2.4. Preparation and optimisation of the active barrier layer

Interfacial polymerisation was carried out to form a polyamide active barrier layer on the NNC scaffolds. The aqueous phases were prepared by dissolving PIP and MPD in DI water, while the organic phase was prepared by dissolving TMC in hexane. As a first step in the optimisation of the barrier layer, different concentrations of monomers [0.25, 0.5, 1.0, 2.0 and 4.0% (w/v)] were chosen to prepare the aqueous phases, while different concentrations of TMC [0.1, 0.2 and 0.4% (w/v)] were chosen for the organic phase. The second step of optimisation involved an investigation of different reaction times for the formation of the polyamide layer. The NNC scaffolds were immersed in the aqueous phase for 1, 3 or 5 min and then immersed in the organic phase for 10 s, 30 s, 1 min, 3 min or 5 min. The third step of optimisation was the investigation of the crucial drying time for the two phases. The NNC scaffolds were immersed in the aqueous phase and then left in air for 2.5, 5, 7.5 and 10 min. Moreover, two different methods were performed in the third step: (1) the scaffolds were wetted with aqueous solutions and immediately immersed in the organic solution without drying; and (2) a rubber roller was used to remove excess aqueous solution from the surface of scaffold before it was immersed in the organic solution. The last step of optimisation of the barrier layer involved the use of further processes to complete the crosslinking of the polyamide layer. The organic solution was drained out and the thin layered NNC scaffolds (TFNC) were cured at ≈21 (room temperature), 65, 70, 90 or 110°C for 10 min each. The final TFNC membranes were washed and stored in DI water until testing.

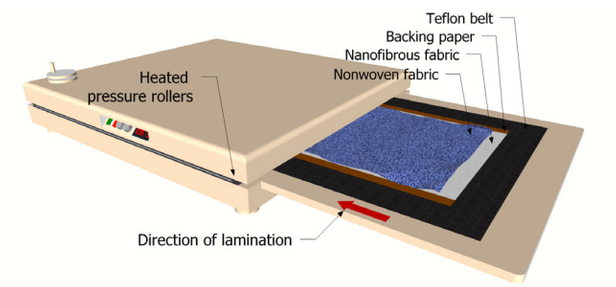

Fig. 2. Lamination of nanofibrous and nonwoven fabric using RPS-Mini fusing lamination equipment.

2.5. Evaluation of the TFNC membrane performance

A dead-end solvent-resistant stirred cell (Millipore-XUF 047 01) with an active filtration area of 15 cm^2 and capacity of 0.05 L was used for evaluation of the membrane performance. The aqueous feed solutions were prepared using NaCl or $MgSO_4$ salts separately (2000 ppm). The feed chamber was pressurised with nitrogen gas and tests were conducted at room temperature (≈21°C) at an applied pressure of 4.8 bar. A sufficient volume of DI water was passed through the TFNC membrane before testing to ensure stable membrane performance. The conductivity of permeates was measured using a digital conductivity meter. The rejection was calculated using Eq. (1).

$$\text{Rejection (\%)} = \frac{Cf - Cp}{Cf} \times 100 \quad (1)$$

where Cf and Cp are the conductivity of the feed and permeate concentrations.

2.6. Characterisation of the NNC scaffold and TFNC membrane

The NNC scaffold and TFNC membranes were dried at room temperature for 24 h and then coated with a 5 nm layer of gold using a QuorumQ150R ES sputter coater for observing of surface morphologies. The surface morphologies of the NNC scaffold and the MPD and PIP based TFNC membranes were investigated using scanning electron microscopy (Tescan-Vega3 SEM). Cross-section images were also obtained by SEM to observe the regularity of lamination and the thickness of layers. The fibre diameter was measured using NIS-Elements AR (Nikon) computer

software, and the average fibre diameter of 100 different fibres was determined. Attenuated total reflectance fourier transform infrared spectroscopy (ATR-FTIR) characterisations of the NNC scaffold and the MPD- and PIP-based TFNC membrane surfaces were made with an ATR accessory, using a Nicolet IZ10 instrument (Thermo Fisher Scientific Inc., Waltham, MA). Samples were analysed by a reflection technique using a germanium crystal. The surface roughness of the TFNC membranes was analysed using an atomic force microscope (JPK Nano wizard III). Measurements included average roughness (Ra), root mean square (RMS) roughness and peak-to-valley roughness (Rt). The surface hydrophilicity of the NNC scaffold and MPD and PIP based TFNC membranes was evaluated using an optical angle meter (Advex Instruments s.r.o). The contact angle was obtained from measurements of the right and left side angle of water droplets. For each sample, 60 measurements were done in different spots on the samples while the water droplets reached steady state. No differences were found between the right and left angles of a droplet; therefore, the average contact angle was calculated to define the exact value of the contact angle. The NNC scaffold was mechanically tested with a Lab Test 2.050 instrument (LaborTech) and the data were evaluated using Lab Test 3 software. Samples with dimensions of 50 × 25 mm^2 were used for the tensile strength measurements. The pore size distribution (mean flow, bubble point, smallest pore) was determined using a capillary flow porometer. In this method, a wetting liquid is allowed to fill the pores of the NNC materials and then a nonreacting inert gas is allowed to displace the liquid from the pores. The pore size is calculated by:

$$D = 4\gamma \cos\theta / p \quad (2)$$

where D is the pore diameter, γ is the surface tension of the liquid, θ is the contact angle of liquid, and p is the differential gas pressure. The measured gas pressure and flow rates allow calculating of the pore throat diameters, pore size distribution and gas permeability (Porous Materials Inc., USA).

3. Results and discussion

3.1. Characteristics of the NNC scaffolds and TFNC membranes

In this study, PA6 nanofibres were produced on a backing paper substrate using a Nano spider electro spinning equipment. Reasons for the choice of the PA6 polymer was its lower price and its relatively hydrophilic property when compared to other phase inversion polymers. The production of nanofibrous supporting material was continuous, which is one of the advantages of commercial nanospider electrospinning equipment. The PA6 nanofibrous layer was transferred onto a PP/PE spunbond nonwoven layer by the lamination method. Fig. 3 shows SEM images of the top views and cross-sections of the NNC scaffolds.

The average fibre diameter of the NNC scaffold top layer was 126 ± 29.1 nm and its mean flow pore size was 0.739 µm. Further features of the NNC scaffold are listed in Table 1.

The tensile strengths of the nonwoven layer, nanofibrous scaffold and NNC scaffold were tested individually.

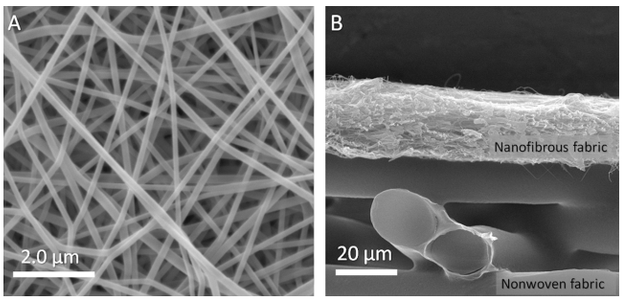

Fig. 3. SEM images of (a) top view (nanofibres) and (b) cross-sectioned NNC scaffolds.

Table 1
Properties of NNC scaffold

	NNC scaffold
Smallest pore size (µm)	0.46
Bubble point pore size (µm)	1.06
Mean flow pore size (µm)	0.73
Fibre diameter (nm)	126 ± 29.1
Non-fibrous area (%)	0.01

The nanofibrous layer showed weak mechanical properties of 4.33 N/25 mm (machine direction) and 4.12 N/25 mm (counter-direction) while the tensile strength of the bi-component spunbond nonwoven layer was 14.95 N/25 mm (machine direction) and 6.14 N/25 mm (counter-direction). After lamination, the tensile strength of the NNC scaffold was increased to 29.17 N/25 mm (machine direction) and 14.42 N/25 mm (counter-direction). The tensile strength tests were indicated that laminated nonwoven and nanofibrous scaffolds performed 4 times higher mechanical strength than nanofibrous layer and 2 times higher mechanical strength than nonwoven fabric. The high mechanical strength of NNC scaffolds was proved the great adhesion between nonwoven and nanofibrous layer. The thicknesses of the nanofibrous scaffold and spunbond bi-component nonwoven layer were 38 ± 0.5 µm and 75 ± 1 µm, respectively. After lamination, the total scaffold thickness was 105 ± 5 µm.

The presence of the PA6 nanofibrous material on the nonwoven supporting surface, and of the interfacial polymerisation of m-phenylenediamine, piperazine and trimesoyl chloride that produced the polyamide active barrier layer structure, was confirmed by ATR-FTIR (Fig. 4). The spectrum of the NNC scaffold surface (Fig.4a) showed a typical polyamide 6, which is based on one single monomer with six carbons. The spectra of the MPD-based membrane (Fig. 4b) showed the absence of the acid chloride band at 1768 cm^{-1} and a strong band at 1654 cm^{-1} (amide I) characteristic of C=O bands of an amide functional group, indicating that successful polymerisation had occurred. Other bands characteristic of aromatic polyamide is also seen at 1540 cm^{-1} (amide II, C=N stretch) and 1606 cm^{-1} (aromatic ring breathing). The spectra of PIP-based membrane (Fig.4c) showed a strong C=O band and an aromatic ring between 1660–1556 cm^{-1}. No aromatic polyamide structure

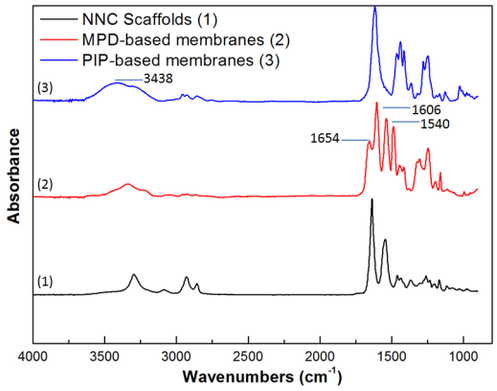

Fig. 4. ATR-FTIR of NNC scaffold (1) and (2) 2.0–0.2 % (w/v) MPD–TMC, (3) 2.0–0.2 % (w/v) PIP–TMC.

was observed between 1573–1508 cm^{-1}, indicating that the PIP-based membrane assumed a more linear chain structure during IP polymerisation.

The most important difference between the PIP-based and MPD-based membranes was the formation of the –COOH group arising from the hydrolysis of the unreacted carbonyl chloride. The –OH (3438 cm^{-1}), which was found in both membranes, confirmed the existence of carboxylic acid. However, the amount of –OH was greater in the PIP-based membrane than in the MPD-based membrane because the reactivity with TMC was lower for PIP than for MPD [32].

Table 2 gives the roughness properties of the NNC scaffold, the MPD-based membrane (2.0 % MPD and 0.2% TMC – 3 min in aqueous and 30 s in organic solutions – 5 min for drying time – 10 min and 65°C for curing time and temperature) and the PIP-based membrane (2.0% PIP and 0.2% TMC – 3 min in aqueous and 30 s in organic solutions – 5 min for drying time – 10 min and 65°C for curing time and temperature). The AFM results indicated that presence of the PA active barrier layer decreased the surface roughness of the NNC scaffold when compared with the MPD- or PIP-based membranes. The roughness values of the MPD-based and PIP-based membranes were almost the same.

The average contact angles of the NNC scaffolds, MPD (2.0% MPD and 0.2% TMC – 3 min in aqueous and 30 s in organic solutions – 5 min for drying time – 10 min and 65°C for curing time and temperature) and PIP (2.0 % PIP and 0.2 % TMC – 3 min in aqueous and 30 s in organic solutions – 5 min for drying time – 10 min and 65°C for curing time and temperature) based membranes are given in Table 3. The NNC scaffold showed a slightly hydrophilic behaviour due to the high degree of surface roughness and the high contact angle, whereas the membranes with the active barrier layer had a more hydrophilic behaviour than the NNC scaffold. The average contact angle of the PIP-based TFNC membranes was 8.2°.

Table 2
AFM properties of specimens

Specimens	NNC scaffold	MPD-based TFNC	PIP-based TFNC
Average roughness (nm)	53.25 ± 5.2	22.45 ± 4.5	18.77 ± 3.8
RMS roughness (nm)	85.17 ± 9.5	27.64 ± 4.9	23.66 ± 4.1
Peak-to-Valley roughness (nm)	298.21 ± 12.1	161.7 ± 9.7	135.1 ± 8.5

Table 3
Contact angle measurement of specimens

Specimens	NNC scaffolds	MPD-based membranes	PIP-based membranes
Average contact angle	62.7°	56.5°	8.2°

3.2. Optimisation and evaluation of the TFNC membranes

The active barrier layer was formed by interfacial polymerisation by introducing an organic solution on top of the NNC (PP-PE/PA6) scaffold containing an aqueous solution. The most important polymerisation parameters for the optimisation of the barrier layer were investigated. The membrane performance (flux and rejection) at each step was used to select one of the optimised conditions and the investigation then proceeded to the next step.

3.2.1. Variation of concentrations of monomer solutions

The first attempt at formation of a barrier layer on the NNC scaffold investigated various concentrations of monomer solutions [0.25, 0.5, 1.0, 2.0 and 4.0% (w/v) aqueous solutions of PIP and MPD and 0.1, 0.2 and 0.4% (w/v) TMC in hexane] at a constant reaction time of 3 min (aqueous solution) and 30 s (organic solution). The drying time after immersion in the aqueous solution was kept constant at 5 min. The final TFNC membrane was cured at 65°C in an oven for 10 min. Fig. 5 shows the top view and cross-sectional images of the barrier layers prepared by the IP method. The reaction of both MPD and PIP monomers with TMC led to the successful formation of a dense layer on the NNC scaffold. The pattern of the nanofibres layer was visible from the surface of the SEM images of TFNC membranes; nevertheless, the PIP-based TFNC membrane clearly formed a defect-free barrier layer while the MPD-based TFNC membrane formed a spotted (dotted) barrier layer.

Fig. 5d shows that an active barrier layer failed to polymerisation or coat the nonwoven fabric without nanofibrous scaffolds. This membrane was performed zero rejection and was not investigated further in this study.

Fig. 6 shows the NF performance (flux and rejection of NaCl/$MgSO_4$) of the IP of MPD-based membranes. Increasing the MPD concentration generally resulted in an increase in the rejection and a decreased flux. The lowest salt rejection was obtained when the TMC concentration was fixed at 0.1% (w/v) because of the lack of crosslinking or the presence of cracks in the barrier layer (Fig. 7a). A concentration of TMC of 0.2% (w/v) gave the highest values for the

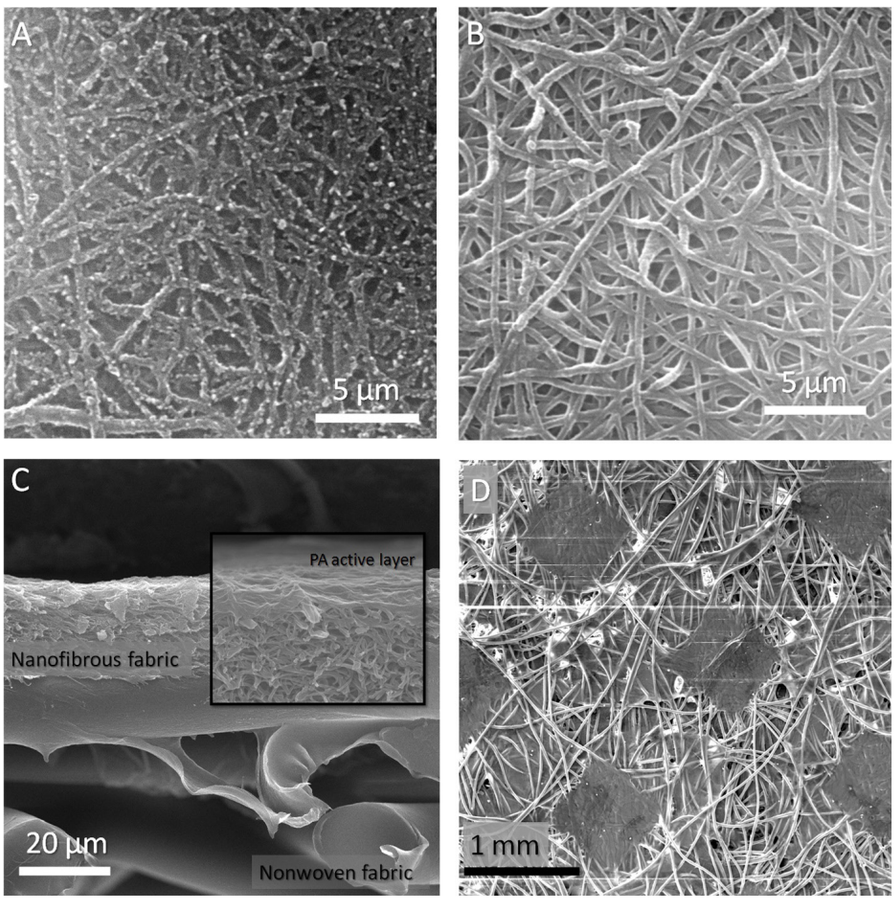

Fig. 5. SEM images of TFNC membranes (a) 2.0–0.2% (w/v) MPD–TMC, (b) 2.0–0.2% (w/v) PIP–TMC, (c) cross-sectioned 2.0–0.2% (w/v) PIP–TMC, (d) Unsuccessful polymerisation of active layer on nonwoven fabric.

rejection performance. For example, the combination of an MPD concentration of 2.0% (w/v) and a TMC concentration of 2.0% (w/v) gave a rejection of 76.5% (NaCl). However, when the TMC concentration was fixed at 0.4% (w/v), the rejection decreased dramatically. The flux obtained with 0.4% (w/v) TMC [and MPD < 2% (w/v)] was higher than that obtained with 0.2 % (w/v) TMC and it was lower [with MPD 2–4 % (w/v)] than that obtained with 0.2% (w/v) TMC (Table 4). The reason for the higher flux and lower rejection in the initial TFNC membranes with a TMC concentration of

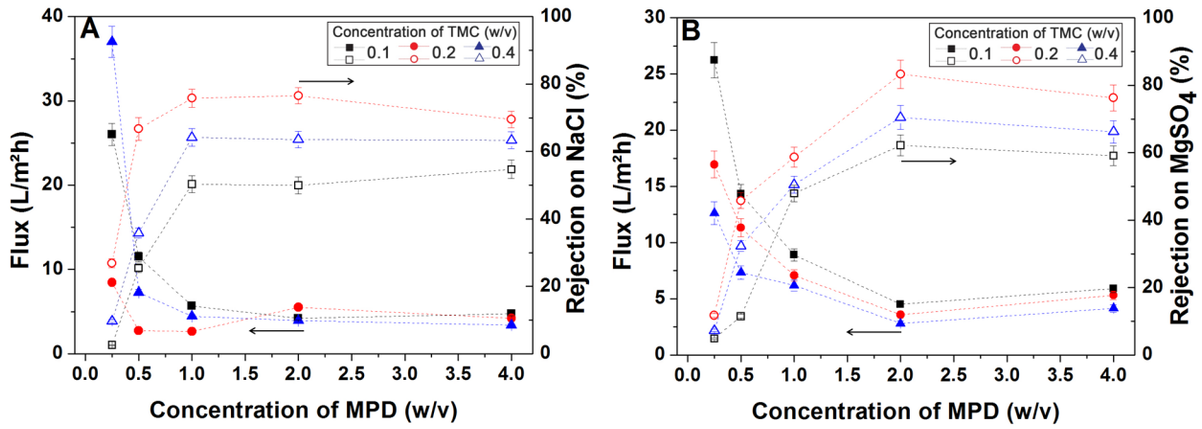

Fig. 6. Dependence of the flux and rejection on MPD concentration for various TMC concentrations with TFNC-based membranes using feed solutions of 2000 ppm (a) NaCl and (b) $MgSO_4$.

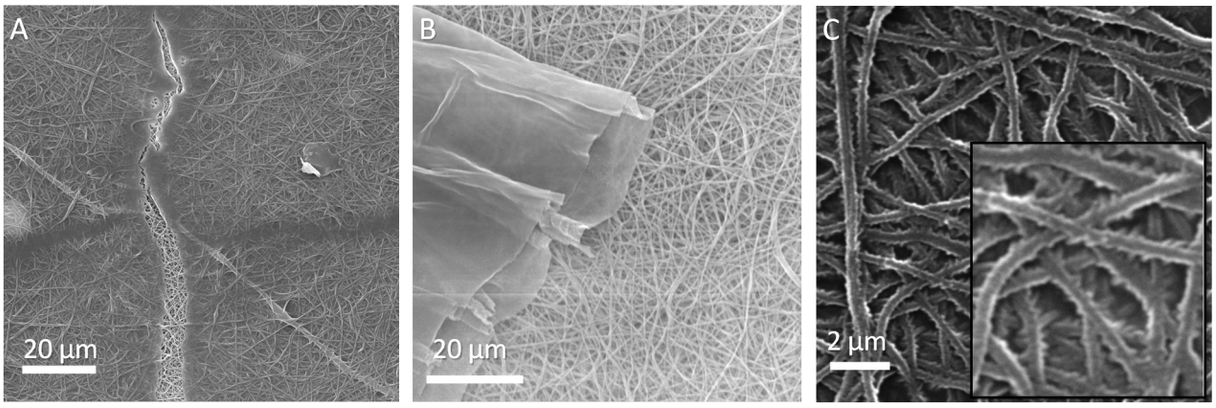

Fig. 7. A crack (a) and an unformed active layer (b) on the NNC scaffold; (c) thorn-like structures on the active layer.

0.4% (w/v) was that they had a higher acid chloride concentration and an insufficient amine concentration. Hence, the IP reaction created a defective PA active layer. The reason for the lower flux and rejection of the TFNC membranes with a TMC concentration of 0.4% (w/v) was that the higher ratio of MPD [2–4 % (w/v)] could increase amount of amine which tended to diffuse into the organic phase on the NNC scaffold during the IP reaction. Hence, the thickness of the barrier layer increased while the flux performance decreased. The thickness of the PA active layers of MPD-based [2.0 MPD – 0.2 TMC and 2.0 MPD – 4.0 TMC % (w/v)] are shown in Fig. 8. The thickness of PA active layer of 2.0 MPD – 0.2 TMC based membrane was 583.57 nm whereas the thickness of PA active layer of 2.0 MPD – 4.0 TMC based membranes was 961.08 nm. A higher amine or acid chloride concentration also could result in the loose formation skin having brittle and disordered active barrier layers, which were allowed greater passage of salt ions [33]. Sundet has reported that there is optimum level for amine and acid chloride concentration to obtain optimum rejection and flux performance [34]. A high $MgSO_4$ rejection of 83.2% was obtained with the combination of 2.0% (w/v) MPD and 0.2%(w/v) TMC.

The NF performances of the IP of PIP-based membranes are shown in Fig. 9. The same flux and rejection trends were

Table 4
Flux and rejection performance of MPD and PIP based membranes

Concentration of MPD-TMC (w/v)%		Flux (L m^{-2} h^{-1})		Rejection (%)		Concentration of PIP-TMC (w/v)%		Flux (L m^{-2} h^{-1})		Rejection (%)	
		NaCl	$MgSO_4$	NaCl	$MgSO_4$			NaCl	$MgSO_4$	NaCl	$MgSO_4$
0.25		26.1	23.8	2.5	14.7	0.25		757.5	650.1	1.8	2.9
0.5		11.4	10.2	25.3	29.5	0.5		158.7	185.1	3.6	5.7
1.0	0.1	5.6	6.1	50.3	56.2	1.0	0.1	132.8	85.2	5.6	16.9
2.0		4.2	4.5	49.9	62.1	2.0		64.2	82.7	7.5	63.8
4.0		4.7	5.9	54.7	59.1	4.0		67.4	77.8	10.4	74.5
0.25		8.4	9.3	26.8	29.3	0.25		463.8	490.2	3.2	6.2
0.5		2.7	6.2	66.7	72.5	0.5		145.4	117.7	5.3	48.1
1.0	0.2	2.6	3.9	75.8	81.9	1.0	0.2	120.4	65.5	17.2	59.6
2.0		5.5	3.5	76.5	83.2	2.0		51.2	59.3	26.3	82.7
4.0		4.2	5.3	69.5	76.5	4.0		48.2	42.5	25.9	80.6
0.25		37.1	11.7	9.7	21.4	0.25		126.6	251.6	2.4	8.1
0.5		7.2	6.8	35.8	45.9	0.5		86.8	102.5	5.3	42.1
1.0	0.4	4.4	5.2	64.1	67.7	1.0	0.4	66.3	49.4	15.3	57.3
2.0		3.9	2.8	63.5	70.4	2.0		49.8	40	15.5	82.2
4.0		3.3	4.1	63.3	66.2	4.0		41.9	44.2	20.4	80.1

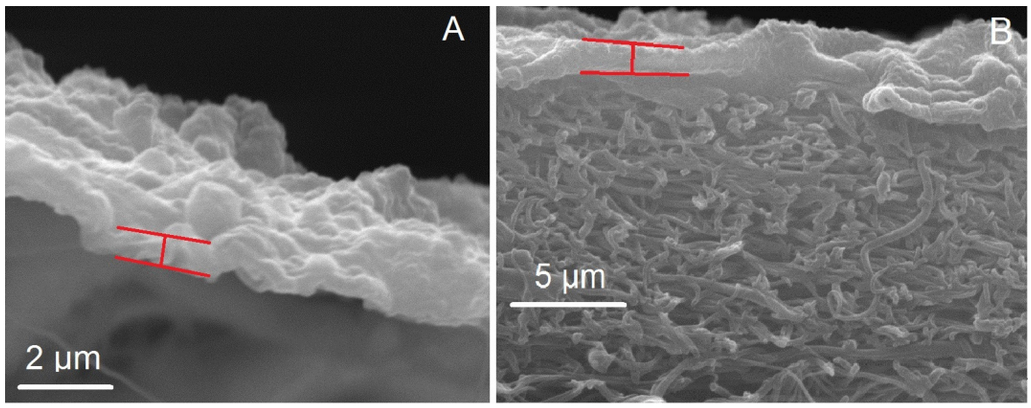

Fig. 8. Cross-sectioned images of (a) 2.0 MPD – 2.0 TMC based and (b) 2.0 MPD – 4.0 TMC based membranes.

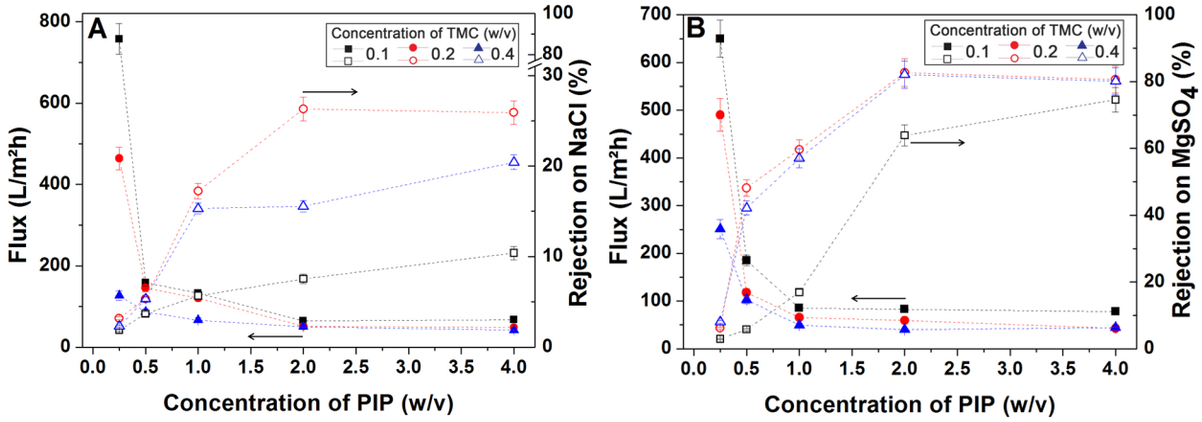

Fig. 9. The dependence of flux and rejection on PIP concentration at various TMC concentrations in TFNC-based membranes using feed solutions of 2000 ppm (a) NaCl and (b) MgSO4.

seen with the MPD-based membranes also obtained with the PIP-based membranes. The PIP-based membranes showed more or less the same rejection performance as the MPD-based membranes for rejection of $MgSO_4$, but the rejection of NaCl, shown in Fig. 9a, was lower than that shown in Fig. 6a at all concentrations (see also Table 4). The reason for the selectivity of the PIP-based membranes for divalent over monovalent ions is the formation of a charged PA active barrier layer on the NNC scaffolds, which contains pendant carboxylic acid groups (see Fig. 4 – ATR-FTIR). These charged carboxylic acid groups arise due to the partial hydrolysis of unreacted acyl chloride group during the IP reaction. The generally accepted explanation for the selective $MgSO_4$ salt rejection by PIP-based membranes is the contribution of an electrostatic repulsion mechanism rather than a size exclusion mechanism [1,4].

Figs. 6 and 9 indicate another significant difference. The PIP-based TFNC membranes exhibited higher permeate fluxes when compared with the MPD-based TFNC membranes. The reasons for these higher permeate fluxes may be summarised as follows: (1) MPD is a more reactive monomer compared to PIP for the IP reaction. The amine groups in MPD solutions can continually cross the water–hexane interface, diffuse through the already formed polyamide layer, and then come into contact with acyl chloride on the organic solvent side [1,32]. Thus, an MPD-based active barrier layer (around 0.5 to 1.0 μm) could differ significantly in terms of thickness when compared to a layer formed from PIP (less than 0.4 μm). The presence of a thick active barrier layer on the MPD-based membranes would substantially decrease the permeate flux. The thickness of the PA active layers of MPD and PIP-based [2.0 MPD – 0.2 TMC and 2.0 PIP – 2.0 TMC % (w/v)] are shown in Fig. 10. (2) The contact angle of PIP-based membranes indicated a highly hydrophilic performance when compared with MPD-based membranes. This was due to the linear portion of the PIP-based PA active barrier layer, which possesses free –COOH groups. The water resistance of PIP-based membranes was noticeably low and caused a high flux of water across the entire membrane. (3) The increased surface area of the membrane is believed to have increased the flux [4,35]. Electrospun nanofibrous materials exhibit a well-known phenomenon where the numbers of nano rods or nano-protrusions on the nanofibres increase the surface area of the materials [36,37]. Thorn-like structures were apparent in the high magnification SEM images of the nanofibre surface after the IP reaction

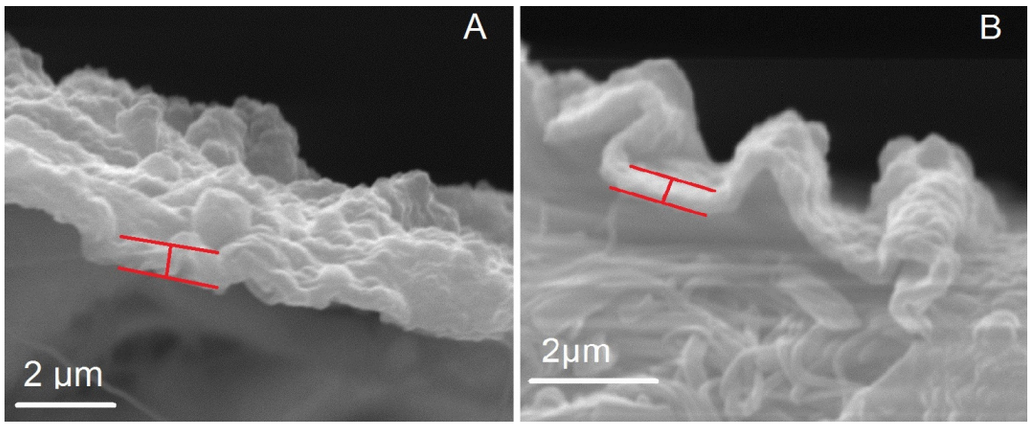

Fig. 10. Cross-sectioned images of (a) 2.0 MPD – 2.0 TMC based and (b) 2.0 PIP – 2.0 TMC based membranes.

of PIP-based membranes (Fig 7c). The directions of these thorn-like protrusions were both horizontal and vertical and they moved inward into the nanofibrous layer. Hence, we assume that the thorn-like structures increased the surface area of PIP-based membranes and provided more opportunities for contact with water, thereby paving the way for enhanced water permeability.

The data presented in Table 4 and Figs. 6 and 9 were analysed to choose the optimum result from the first tests. The combination of 2.0% (w/v) MPD and 0.2 % (w/v) TMC was chosen as the optimum concentrations and was used in all further optimisation and filtration experiments for NaCl feed solution because of the high rejection of monovalent salts (76.5%, NaCl). The combination of 2.0% (w/v) PIP and 0.2% (w/v) TMC concentrations gave a membrane with a rejection rate of 83.2% ($MgSO_4$), while its flux was 59.3 L m^{-2} h^{-1}. The combination of 2.0% (w/v) PIP with 0.2% (w/v) TMC was chosen as the optimum concentration and used in all further optimisation experiments and filtration experiments using $MgSO_4$ feed solution because of the high rejection of divalent salts.

3.2.2. Reaction time in monomer solutions (contact time)

After determination of the optimum concentrations for the TFNC membrane, the second most important parameter was investigated, namely the contact time or reaction time of the NNC scaffold in the monomer solutions. Immersion times of 1, 3 and 5 min were chosen for the aqueous solution and 10 and 30 s and 1, 3, and 5 min for the organic solutions. The drying time after immersion in the aqueous solution was kept constant at 5 min. The final TFNC membranes were cured at 65°C in an oven for 10 min.

Fig. 11 shows the NF performance of MPD-based membranes produced at different reaction times in the solutions. The flux performance increased and rejection performance decreased as the reaction times of MPD and TMC increased. The highest value for rejection of the NaCl feed solution was obtained for the shortest reaction time with both monomers. The TFNC membrane produced by the reaction of 1 min in MPD and 30 s in TMC solutions had a flux of 2.57 L m^{-2} h^{-1} (NaCl) and rejection of 89.5%. The reaction time for the membrane produced after 1 min in MPD and 30 s in TMC was chosen as the optimum and used for the step of curing temperature.

Fig. 12 presents the NF performance of PIP-based membranes produced at different reaction times. The reaction time in both phases had a significant influence on the flux and rejection performance of TFNC membranes. The expected well-known phenomenon of decreasing flux and increasing rejection was not observed. Fig. 12a shows that the flux performance decreased as the reaction times of PIP and TMC increased. However, Fig. 12b shows that an increased in the reaction time with TMC enhanced the rejec-

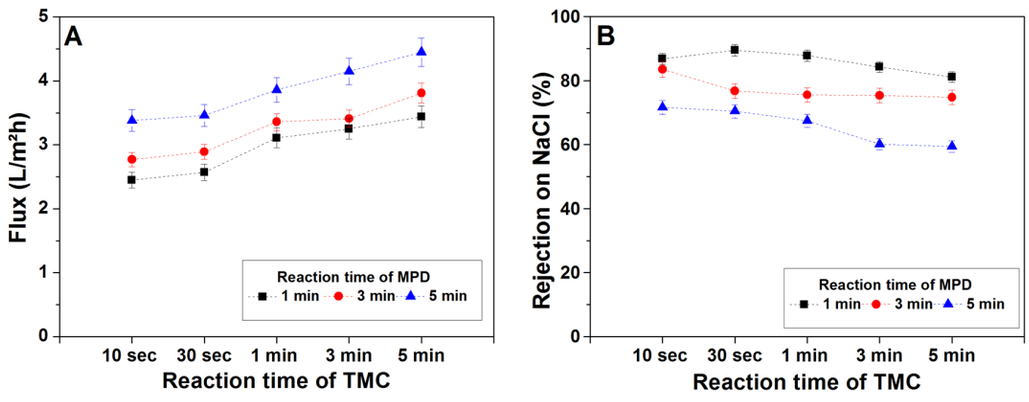

Fig. 11. The reaction time dependence of (a) flux and (b) rejection of MPD-based TFNC membranes using NaCl feed solutions.

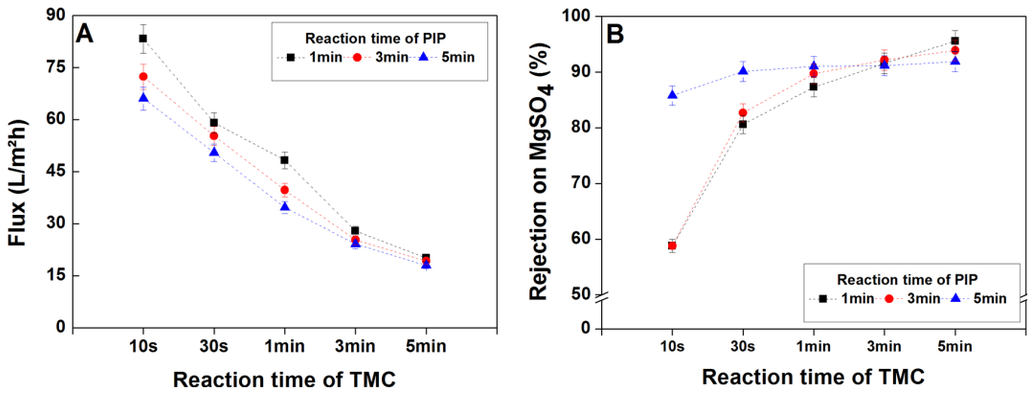

Fig. 12. The reaction time dependence of (a) flux and (b) rejection of PIP-based TFNC membranes using$MgSO_4$ feed solutions.

tion performance of TFNC membranes, whereas increases in the reaction time with PIP first affected the rejection performance positively (at 10s, 30s, and 1 min for TMC) and then negatively (at 3 and 5 min for TMC). For example, the TFNC membrane reacted for 5 min in PIP and TMC solutions had a flux of 16.5 L m^{-2} h^{-1} ($MgSO_4$) and rejection of 91.9%, while the TFNC membrane immersed for 1 min in PIP solution and for 5 min in TMC solution had a flux of 20.2 L m^{-2} h^{-1} ($MgSO_4$) and rejection of 95.6%. The increased reaction time for both solutions led to excessive crosslinking of the monomers and formation of a thicker active barrier layer on the TFNC membrane surface, which decreased the flux performance. Excessive crosslinking also disrupted the structure of the active barrier layer, thereby decreasing its selectivity. The results shown in Fig. 12a, b indicated the possibility of an enhancement of the rejection performance without compromising the flux performance of the TFNC membranes. The reaction times of 5 min in PIP solution and 30 s in TMC solution were chosen as the optimum reaction times because of the reasonable rejection and high flux performance (90.1% and 50.5 L m^{-2} h^{-1}, $MgSO_4$, respectively) obtained and were used for the next step.

Figs. 11 and 12 confirm the higher reactivity of MPD monomers than PIP monomers with TMC, as indicated by the highest values of rejection with short reaction times. The PIP monomer needed a longer time to react with TMC to obtain high rejection values.

3.2.3. Determination of the drying method and time

The drying time is one of the most important parameters of the fabrication of TFNC membranes. Following the immersion of the NNC scaffold in aqueous monomer solution (PIP or MPD), the nascent TFNC membranes had to be held vertically to remove excess monomer solution. The PIP-based membranes and $MgSO_4$ feed solution were used to determine the drying method and time because of their higher flux performance. Different process conditions, enumerated from 1 to 6, were chosen for evaluation of their filtration performance, which is shown in Table 5. In this Table, (1) represents the PIP-solution-wetted nascent scaffold was immersed in TMC solution immediately, without a drying process. In this case, the barrier layer did not attach to or properly cover the nanofibre surface (Fig. 7b) and achieved zero rejection and excessive flux (Table. 5). The process of squeezing excessive PIP solution from nascent NNC scaffold using a rubber roller caused the formation of an active barrier layer that showed selectivity (2).

The rejection performance of TFNC membranes increased when the drying time was increased up to 5 min. After 5 min, the rejection performances decreased because the amine groups were unable to cross the water-hexane interface and come into contact with the acyl chloride on the organic solvent side. This was due to the excessive drying of the PIP solution on the nascent NNC scaffolds (5)–(6) shown in Table 5. The flux through the TFNC membranes exhibited an inherently opposite performance to that seen in rejection. Balancing the drying time of the PIP solution – at the so-called 'sweet spot' – is one important condition for the proper formation of the active barrier layer on the NNC scaffold. The optimal value for the drying time for the IP reaction between aqueous and

Table 5
The drying method and time dependence of flux and rejection of PIP-based membranes using feed solutions of 2000 ppm $MgSO_4$

Enumerated drying style	Flux (L m^{-2} h^{-1})	Rejection (%)
1	1356	0
2	57	84.9
3	56.8	86.1
4	53.1	90.2
5	55.7	88.3
6	88.1	65.7

[1]After immersion in PIP solution, the scaffold was immediately immersed in TMC solution.
[2]After immersion in PIP solution, excessive PIP solution was squeezed out with a rubber roller and then the scaffold was immediately immersed in TMC solution.
[3]After immersion in PIP solution, the wetted scaffold was held vertically in air for 2.5 min and then immersed in TMC solution.
[4]After immersion in PIP solution, the wetted scaffold was held vertically in air for 5 min and then immersed in TMC solution.
[5]After immersion in PIP solution, the wetted scaffold was held vertically in air for 7.5 min and then immersed in TMC solution.
[6]After immersion in PIP solution, the wetted scaffold was held vertically in air for 10 min and then immersed in TMC solution.

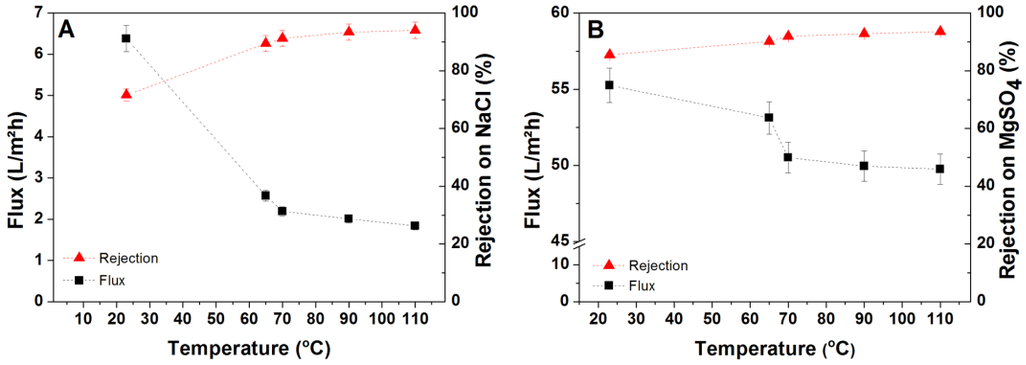

Fig. 13. The temperature dependence of flux and rejection of (a) MPD-based membranes using feed solutions of 2000 ppm NaCl, (b) PIP-based membranes using feed solutions of 2000 ppm $MgSO_4$.

organic solutions was determined as 5 min and was used int he final step for both PIP and MPD solutions.

3.2.4. Determination of the curing temperature

The TFNC membranes need a curing process to complete the crosslinking of the barrier layer. This process is essentially the last step in the formation of the active barrier layer on the NNC scaffolds when there is no additional post-treatment. Following the immersion of the nascent TFNC scaffold into the TMC solution, the membranes were placed in the oven at different temperatures of ≈21, 65, 70, 90 and 110°C for 10 min. This treatment not only dries and anneals the film but also performs the crucial step of crosslinking the residual unformed active barrier layer. The temperature was not set higher than 110°C because of the low melting point of PE (around 120–130°C). One membrane was also kept at room temperature after immersion in the TMC solution to observe the effect of no heat treatment on the filtration performance. Fig. 13 shows the flux and rejection performance of TFNC membranes cured at different temperatures. A clear difference was evident between the membranes left at room temperature and those heat-treated at 65°C, as the flux decreased from 6.38 to 2.57 L m^{-2} h^{-1} (NaCl) and the rejection increased from 71.58 to 89.5% after heating. Curing temperature increases from 70 to 90 or 110°C caused slight decreases in the flux of TFNC membranes (2.19, 2.01 and 1.84 L m^{-2} h^{-1}, respectively), whereas the rejection of the membranes increased [91.22, 93.38 and 94.04%, respectively; Fig. 13a].

Fig. 13b shows that a flux decrease from 55.7 to 53.2 L m^{-2} h^{-1} ($MgSO_4$) was accompanied by a rejection increase from 85.7 to 90.22%. A curing temperature increase from 70 to 90 or 110°C resulted in a more or less stable flux (50.51, 49.95 and 49.75 L m^{-2} h^{-1}, respectively), where as the rejection increased (91.95, 92.86 and 93.57%, respectively).

These preliminary results from this study indicate that an optimised active barrier layer based on a well-designed nanofibrous supporting surface is suitable for use in NF membranes for separation of salt (monovalent or divalent) ions without any extra additives or modification processes.

4. Conclusions

Large-scale PA6 nanofibrous scaffolds on the paper backing material were transferred onto PP/PE bi-component spunbond nonwoven fabric using lamination methods to eliminate the disadvantageous factors of nanofibrous scaffolds, such as weak mechanical properties and poor adhesion to the nonwoven surface. The resulting TFNC membrane was able to withstand applied pressure during filtration tests without experiencing any damage to its surface. The nanofibrous material and active barrier layers remained fastened to the nonwoven fabric throughout the tests. The lamination method increased the mechanical properties of NNC scaffold and created a smooth surface for better IP. The optimum active barrier layer was obtained on the NNC scaffold by optimising four different basic production steps. Different concentrations and types of monomers directly affected the rejection and flux performance. MPD-based membranes showed rejection selectivity for monovalent (NaCl) salt ions due to the presence of the aromatic amine structure in the active barrier layer, which made the layer more compact and denser. The PIP-based membranes showed rejection selectivity for divalent ($MgSO_{4)}$ salt ions due to the formation of a charged active barrier layer that contains pendant carboxylic acid groups. The PIP-based membranes showed better flux performance than the MPD-based membranes. The increased flux seen with PIP-based membranes is believed to result from their increased surface area and low contact angle features. The reaction (contact) time and drying time for the NNC scaffold during the IP reaction influenced the thickness and pore size of the active barrier layer and thereby had dramatic effects on the filtration performance. The effect of different curing temperatures revealed the potential of increasing the rejection performance without sacrificing the flux performance. The TFNC membrane performance could be further enhanced with various kind of additives to the solutions (e.g., surfactants, ionic liquids, nanoparticles, acid acceptors) or by surface modification (plasma treatment, surface modifying macromolecules). It is believed that fabrication of TFNC membranes based on laminated NNC scaffolds is promised the suitability of the large-scale industrial production. Further research should be conducted to improve the filtration performance in terms of flux and rejection, including the use of cross-flow filtration equipment to evaluate TFNC membranes.

Acknowledgment

The results of this project LO1201 were obtained through the financial support of the Ministry of Education, Youth

and Sports in the framework of the targeted support of the National Programme for Sustainability I. Special thanks to Dr. Marek Jaromir and Dr. Jana Mullerova for their great help.

Abbreviations

NNC	—	Nonwoven and nanofibrous composite
TFNC	—	Thin film nanofibrous composite
MPD	—	m-phenylenediamine
PIP	—	Piperazine
TMC	—	Trimesoyl chloride
PA	—	Polyamide

References

[1] R.J. Peterson, Composite reverse osmosis and nanofiltration membranes, J. Membr. Sci., 83 (1993) 81.
[2] R.W. Baker, Membrane Technology and Applications, third ed., John Wiley& Sons, Chichester, (2012) 207–247.
[3] T. Matsuura, Progress in membrane science and technology for seawater desalination—a review, Desalination, 134 (2001) 47–54.
[4] V. Freger, Nanoscale heterogeneity of polyamide membranes formed by interfacial polymerization, Langmuir, 19 (2003) 47–91.
[5] Y. Song, P. Sun, L.L. Henry, B. Sun, Mechanisms of structure and performance controlled thin film composite membranes formation via interfacial polymerization process, J. Membr. Sci., 251 (2005) 67–79.
[6] M. Liu, S. Yu, M. Qi, Q. Pan, C. Gao, Impact of manufacture technique on seawater desalination performance of thin-film composite polyamide-urethane reverse osmosis membranes and their spiral wound elements, J. Membr. Sci., 348 (2010) 268–276.
[7] C.C. Wamser, R.R. Bard, V. Senthilathipan, Synthesis and photoactivity of chemically asymmetric polymeric porphyrin films made by interfacial polymerization, J. Am. Chem. Soc., 111 (1989) 8485–8491.
[8] A.K. Ghosh, and E.M.V. Hoek, Impacts of support membrane structure and chemistry on polyamide-polysulfone interfacial composite membranes, J. Membr. Sci., 336 (2009) 140–148.
[9] C.K. Kim, J.H. Kim, I.J. Roh, J.J. Kim, The changes of membrane performance with polyamide molecular structure in the reverse osmosis process, J. Membr. Sci., 165 (2000) 189–199.
[10] Y. Jin, and Z. Su, Effects of polymerization conditions on hydrophilic groups in aromatic polyamide thin films, J. Membr. Sci., 330 (2009) 175–179.
[11] Y. Mansourpanah, S.S. Madaeni, A. Rahimpour, Fabrication and development of interfacial polymerized thin-film composite nanofiltration membrane using different surfactants in organic phase; study of morphology and performance, J. Membr. Sci., 343 (2009) 219–228.
[12] L. Yung. H. Ma, X. Wang, K. Yoon, R. Wang, B.S. Hsiao, B. Chu, Fabrication of thin-film nanofibrous composite membranes by interfacial polymerization using ionic liquids as additives, J. Membr. Sci., 265 (2010) 52–58.
[13] M. Hirose, H. Ito, Y. Kamijama, Effect of skin layer surface structures on the flux behavior of RO membranes, J. Membr. Sci., 121 (1996) 209–215.
[14] A.K. Ghosh, B.H. Jeong, X. Huang, E.M.V. Hoek, Impacts of reaction and curing conditions on polyamide thin films, J. Membr. Sci., 330 (2009) 175–179.
[15] T.H. Grafe, K.M. Graham, Nanofiber webs from electrospinning. Nonwovens in Filtration—Fifth Int. Conf. (2003) 1–5.
[16] D. Emig, A. Klimmek, E. Raabe, Dust filter bag containing nano nonwoven tissue, US Patent 6,395,046 B1.
[17] M.G. Hajra, K. Mehta, G.G. Chase, Effects of humidity, temperature, and nanofibers on drop coalescence in glass fiber media, Sep. Purif. Technol., 30 (2003) 79–98.
[18] C. Shin, G.G. Chase, Water-in-oil coalescence in micro-nanofiber composite fibers, AIChE J., 50 (2004) 343–350.
[19] L. Raghuraman, Membrane material for brackish-water application for utilities—an evaluation, Desalination, 91 (1993) 155–162.
[20] I. Koyuncu, M. Yazgan, Application of nanofiltration and reverse osmosis membranes to the salty and polluted surface water, J. Environ. Sci. Health Part A: Tox./Hazard. Subst. Environ. Eng., 36 (2001) 1321–1333.
[21] I.J. Roh, and V.P. Khare, Investigation of the specific role of chemical structure on the material and permeation properties of ultrathin aromatic polyamides, J. Mater.Chem., 12 (2002) 23–34.
[22] A.P. Rao, S.V. Joshi, J.J. Trivedi, C.V. Devmurari, V.J. Shah, Structure–performance correlation of polyamide thin film composite membranes: effect of coating conditions on film formation, J. Membr. Sci., 211 (2003) 13.
[23] C. Fritzmann, J. Löwenberg, T. Wintgens, T. Melin, State-of-the-art of reverse osmosis desalination, Desalination, 216 (2007) 1–76.
[24] S. Kaur, D. Rana, T. Matsuura, S. Sundarrajan, S. Ramakrishna, Preparation and characterization of surface modified electrospun membranes for higher filtration flux, J. Membr. Sci., 390/391 (2012) 235–242.
[25] S. Kaur, R. Barhate, S. Sundarrajan, T. Matsuura, S. Ramakrishna, Hot pressing of electrospun membrane composite and its influence on separation performance on thin film composite nanofiltration membrane, Desalination, 279 (2011) 201–209.
[26] S. Kaur, S. Sundarrajan, D. Rana, T. Matsuura, S. Ramakrishna, Influence of electrospun fiber size on the separation efficiency of thin-film nanofiltration composite membrane. J. Membr. Sci., 392 (2012) 101–111.
[27] K. Yoon, B.S. Hsiao, B. Chu, High flux nanofiltration membranes based on interfacially polymerized polyamide barrier layer on polyacrylonitrile nanofibrous scaffolds, J. Membr. Sci., 326 (2009) 484–492.
[28] X. Wang, T.M. Yeh, Z. Wang, R. Yang, R. Wang, et al. Nanofiltration membranes prepared by interfacial polymerization thin-film nanofibrous composite scaffold, Polymer, 55 (2014) 1358–1366.
[29] L. Yung, H. Ma, X. Wang, K. Yoon, R. Wang, et al. Fabrication of thin-film nanofibrous composite membranes by interfacial polymerization using ionic liquids as additives, J. Membr. Sci., 365 (2010) 52–58.
[30] L. Huang, S.S. Manickam, J.R. McCutcheon, Increasing strength of electrospun nanofiber membranes for water filtration using solvent vapor, J. Membr. Sci., 436 (2013) 213–220.
[31] K. Yoon, B.S. Hsiao, B. Chu, Formation of functional polyethersulfone electrospun membrane for water purification by mixed solvent and oxidation processes, Polymer, 50 (2009) 2893–2899.
[32] R. Lo, A. Bhattacharya, B. Ganguly, Probing the selective salt rejection behavior of thin film composite membranes: A DFT study, J. Membr. Sci., 436 (2013) 90–96.
[33] D.J. Mohan, and L. Kullová, A study on the relationship between preparation condition and properties/performance of polyamide TFC membrane by IR, DSC, TGA, and SEM techniques, Desalin. Water Treat., 51 (2013) 586–596.
[34] S.A. Sundet, Multilayer reverse osmosis membrane in which one layer is poly-metaphenylene-cyclohexane-1,3,5-tricaboxamide, US Patent 4,643,829, February 1987.
[35] S.Y. Kwak, S.G. Jung, S.H. Kim, Structure-motion-performance relationship of flux-enhanced reverse osmosis (RO) membranes composed of aromatic polyamide thin films, Environ. Sci. Technol., 35(2001) 4334–4340.
[36] R. Ostermann, D. Li, Y. Yin, J.T. McCann, Y. Xia, V_2O_5 Nanorods on TiO_2 nanofibers: A new class of hierarchical nanostructures enabled by electrospinning and calcination, Nano Lett., 6 (2006) 1297–1302.
[37] D. Kim, A. Rothschild, B.H. Lee, D.Y. Kim, S.M. Jo, H.L. Tuller, Ultrasensitive chemiresistors based on electrospun TiO_2 Nanofibers, Nano Lett., 6 (2006) 2009–2013.